

# Revisions to Some Parameters Used in Stochastic-Method Simulations of Ground Motion

by David M. Boore and Eric M. Thompson

**Abstract** The stochastic method of ground-motion simulation specifies the amplitude spectrum as a function of magnitude ( $M$ ) and distance ( $R$ ). The manner in which the amplitude spectrum varies with  $M$  and  $R$  depends on physical-based parameters that are often constrained by recorded motions for a particular region (e.g., stress parameter, geometrical spreading, quality factor, and crustal amplifications), which we refer to as the seismological model. The remaining ingredient for the stochastic method is the ground-motion duration. Although the duration obviously affects the character of the ground motion in the time domain, it also significantly affects the response of a single-degree-of-freedom oscillator. Recently published updates to the stochastic method include a new generalized double-corner-frequency source model, a new finite-fault correction, a new parameterization of duration, and a new duration model for active crustal regions. In this article, we augment these updates with a new crustal amplification model and a new duration model for stable continental regions. Random-vibration theory (RVT) provides a computationally efficient method to compute the peak oscillator response directly from the ground-motion amplitude spectrum and duration. Because the correction factor used to account for the nonstationarity of the ground motion depends on the ground-motion amplitude spectrum and duration, we also present new RVT correction factors for both active and stable regions.

*Online Material:* Files of coefficients for evaluating distance ( $D_{\text{rms}}$ ), time-domain-to-random-vibration ratios, and SMSIM parameter files.

## Introduction

The stochastic method is widely used to compute ground motions at frequencies of engineering interest. Since its introduction by [Hanks and McGuire \(1981\)](#) and the enhancements to the method described by [Boore \(1983\)](#), the method has been extended to model stochastic finite-fault effects ([Beresnev and Atkinson, 1998](#); [Motazedian and Atkinson, 2005](#)), deterministic finite-fault effects at low frequencies to produce hybrid stochastic–deterministic simulations ([Frankel, 2009](#); [Graves and Pitarka, 2010](#)), and equivalent-linear site response ([Rathje and Ozbey, 2006](#); [Kottke and Rathje, 2008](#)). All of these applications rely on the stochastic method’s point-source formulation, which has changed little in the last 30 years.

Several modifications and additions to some of the parameters used in many applications of the point-source stochastic method have recently been developed, including a generalized double-corner-frequency (DCF) source model, a modified point-source distance to account for finite-fault effects, a new parameterization of duration for use in the stochastic method, and a new path-duration model for tectonically active crustal regions (ACRs). These adjustments motivate the additional up-

dates that we present here, which include small modifications to the crustal amplifications for rock and very-hard-rock sites, a new path-duration model for stable continental regions (SCRs), and new empirical correction factors for the random-vibration theory (RVT). In addition, we briefly discuss an alternative to the root mean square (rms)-to-peak factor used in the random-vibration (RV) estimates of ground-motion intensity measures (GMIMs). The updates to the RVT provide new coefficients for the equations developed by [Boore and Thompson \(2012\)](#) that give the durations to be used in computing the rms of the oscillator responses in RV simulations. We first discuss parameters that are relevant both to time-domain (TD) and RV simulations of GMIMs, and then we present material specific to the RV simulations.

For convenience, we refer to our results as being applicable to ACRs and SCRs. The notations ACR and SCR are commonly used to differentiate between the two tectonic environments (e.g., [Stewart et al., 2014](#)), but the notation is clearly only an approximation. The data we used to derive the path durations for ACRs are from the Next Generation Attenuation (NGA)-West 2 database, which contains data from

around the world, although the bulk of the data is from western North America (more specifically, the coastal region of California). In this sense, our use of ACR rather than western North America (WNA) might have some justification. For our SCR path durations, however, the data are from eastern North America (ENA). In lieu of data from other SCRs and in keeping with the differentiation of our results into two tectonic regions, we prefer to use ACR and SCR rather than the common terms ENA and WNA (in which “eastern” North America also includes central North America).

### Parameters for Both Time-Domain and Random-Vibration Simulations

#### Generalized Source Model

A number of models for the shape and magnitude scaling of the source spectra are included in the implementation of the stochastic method in the Stochastic-Method SIMulation (SMSIM) program (Boore, 2005). These include single-corner-frequency (SCF) and DCF models. Until recently, the high-frequency spectral level in all but one of the DCF models was determined only by the seismic moment. A generalization of the DCF model (Boore, Di Alessandro, and Abrahamson, 2014) now allows the high-frequency spectral level to be determined by a stress parameter, in addition to the seismic moment.

#### Adjustment of Distance for Finite-Fault Effects

The stochastic method as implemented in SMSIM fundamentally assumes a point representation of the source. Although the basic subroutines in SMSIM or modifications of those subroutines have been used to calculate the motions from the point sources into which finite faults are often decomposed (e.g., Motazedian and Atkinson, 2005; Frankel, 2009; Graves and Pitarka, 2010), it is possible to capture the essential aspects of motions from a finite fault in a single point-source simulation by the use of an appropriate point-source (PS) distance  $R_{PS}$ . This approach is based on the recognition that most of the energy arriving at a site will come from parts of the fault more distant than the closest point on the rupture surface ( $R_{RUP}$ ) (e.g., Baltay and Hanks, 2014). It is clear that  $R_{RUP}$  should not be used in the simulations (as has been done often in the past), because doing so leads to unreasonably large motions close to faults that are not observed in data (e.g., Boore, 2014). A number of modifications to the source-to-site distance have been used (e.g., Atkinson and Silva, 2000; Toro, 2002; Atkinson and Boore, 2003; Boore, 2009; Boore, Di Alessandro, and Abrahamson, 2014; Yenier and Atkinson, 2014; Yenier, 2015). For example, Boore (2009) introduced an effective point-source distance, called  $R_{EFF}$ , that is similar to the rms distance from a site to the rupture surface. This version of  $R_{PS}$  has the disadvantage that it is based on a specific source and site geometry. More general versions of  $R_{PS}$  have been defined recently by Boore, Di Alessandro, and Abrahamson (2014), Yenier and

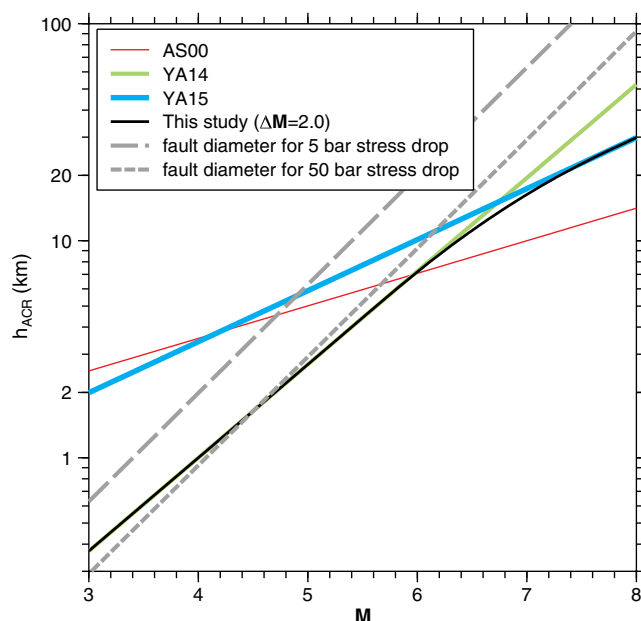


**Figure 1.** Finite-fault factor for active crustal regions (ACRs) ( $h_{ACR}$ ) versus moment magnitude ( $M$ ) proposed by Atkinson and Silva (2000; AS00), Yenier and Atkinson (2014; YA14), Yenier and Atkinson (unpublished report, 2015, see Data and Resources; YA15), and this study. For reference, the fault diameters for two values of stress drop are also shown. The color version of this figure is available only in the electronic edition.

Atkinson (2014), and Yenier (2015). Those studies use the definition of  $R_{PS}$  introduced by Atkinson and Silva (2000),

$$R_{PS} = \sqrt{R_{RUP}^2 + h^2}, \quad (1)$$

with  $h$  being a function of  $M$ , as given by the equation

$$\log h = \alpha + \beta M, \quad (2)$$

in which the logarithm is base 10. Note that  $h$  is not directly related to the depth of the earthquake, even though it appears in equation (1) as if it were a depth. In equation (1), depth is implicitly included in  $R_{RUP}$ . To avoid confusion, we prefer to call  $h$  a finite-fault factor rather than a pseudodepth. Several sets of the coefficients  $\alpha$  and  $\beta$  have been proposed; Figure 1 shows the magnitude dependence of the finite-fault factor for some of these relations. We have added the subscript ACR to  $h$  in recognition of the region from which the data used to obtain the relations were obtained. The Yenier (2015; YA15) relation is loosely constrained by data from a small number of earthquakes with moment magnitudes between 4.0 and 7.6. The Yenier and Atkinson (2014; YA14) relation fits the  $h_{ACR}$  values determined from larger magnitude data better than does the YA15 relation (see fig. 3.3 in Yenier, 2015), but the YA14 relation leads to an oversaturation of short-period ground motions (amplitude scales

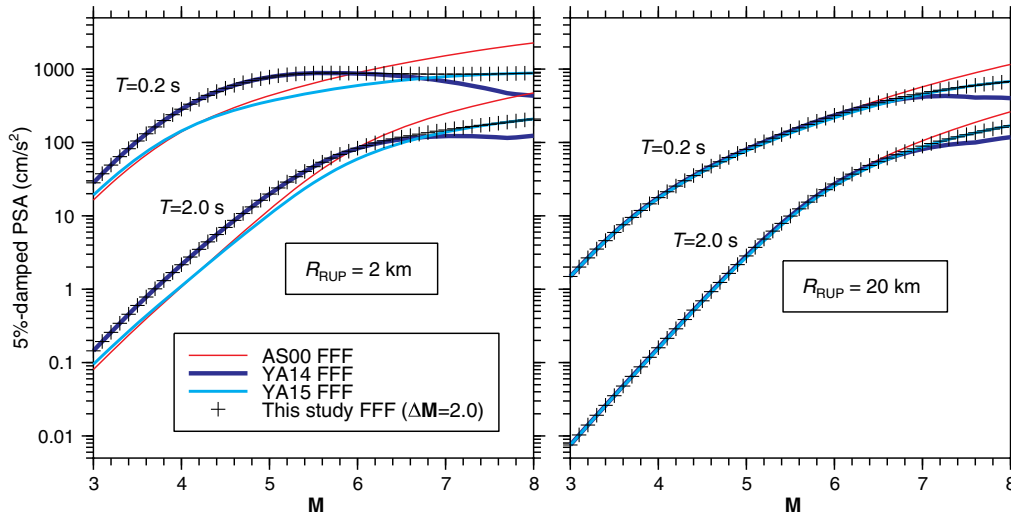


**Figure 2.** Pseudospectral acceleration (PSA) versus moment magnitude ( $M$ ) for the ACR model described in the [Ⓔ](#) electronic supplement, using the finite-fault factors (FFF) shown in Figure 1. The results are shown for rupture distances ( $R_{RUP}$ ) of 2 and 20 km and periods ( $T$ ) of 0.2 and 2.0 s. The color version of this figure is available only in the electronic edition.

inversely with  $M$ ) at short distances to the fault, as shown in Figure 2. It was to prevent such oversaturation that YA15 modified their equation for  $h_{ACR}$ . Although recent ground-motion data suggests that such oversaturation might exist

YA15 lines by a cubic polynomial with coefficients chosen to equal the values and slopes of the lines at either end of a transition range of magnitudes. This results in the following equation for  $h$ :

$$h(M) = \begin{cases} a_1 + b_1(M - M_{t1}) & M \leq M_{t1} \\ c_0 + c_1(M - M_{t1}) + c_2(M - M_{t1})^2 + c_3(M - M_{t1})^3 & M_{t1} < M < M_{t2} \\ a_2 + b_2(M - M_{t2}) & M \geq M_{t2} \end{cases} \quad (3)$$

(e.g., Boore, Stewart, *et al.*, 2014), it is our understanding that most practitioners are reluctant to allow such oversaturation at this time.

One criticism we have of the YA15 relation is that  $h_{ACR}$  for small magnitudes is much larger than the fault size for those magnitudes, for any reasonable range of stress drops. This is shown in Figure 1, in which we have included curves of fault diameter for stress-drop values of 5 bars, which we consider to be a lower limit, and 50 bars, which is a reasonable value for an average stress drop for ACR earthquakes (Baltay and Hanks, 2014). A value of  $h_{ACR}$  significantly greater than a fault dimension for a given magnitude is inconsistent with the interpretation of  $h_{ACR}$  as a finite-fault effect.  $h_{ACR}$  from YA15 is greater than the fault diameters for a 5-bar stress drop for magnitudes less than about 4.8, whereas  $h_{ACR}$  from YA14 is not inconsistent with the fault diameters for a 50-bar stress drop. To take advantage of the smaller values of  $h_{ACR}$  predicted by YA14 at small magnitudes and the YA15 values for larger magnitudes, we suggest a hybrid relation given by combining the YA14 and YA15 relations for  $h_{ACR}$ . To avoid the sharp kink in magnitude scaling of ground motions at a fixed small distance when the two relations are used (e.g., the scaling of pseudospectral acceleration [PSA] in Fig. 2 for  $R_{RUP} = 2$  km), we join the YA14 and

The Appendix gives the equations for computing the  $c$  coefficients from the YA14 and YA15 coefficients. Table 1 gives the coefficients when lines 1 and 2 are given by the YA14 and YA15 relations (the  $a$  and  $b$  coefficients for the two lines on either side of the cubic are given in the first and third rows, respectively) and a transition range of  $M_{t2} - M_{t1} = 2$ , centered on the magnitude at which the two lines intersect (6.74); this transition range was chosen subjectively to give a reasonable, but not excessive, amount of smoothing. We suggest that  $h_{ACR}$  be given by equation (3), with the appropriate coefficients (in contrast to the recommendation in Boore, Di Alessandro, and Abrahamson, 2014, that the YA14 relation be used).

Because earthquakes in SCRs might have higher stress drops than those in ACRs, we would expect the source dimensions, and thus the  $h$  for SCR earthquakes, to be smaller than the earthquakes used in developing equation (3) for earthquakes of the same moment magnitude. One way to derive  $h_{SCR}$  is to use the scaling of source radius as the inverse cube root of stress drop to obtain the relation

$$h_{SCR} = (\Delta\sigma_{ACR}/\Delta\sigma_{SCR})^{1/3} h_{ACR}. \quad (4)$$

Substituting  $\Delta\sigma_{ACR} = 88$  bars (the stress parameter corresponding to the high-frequency spectral level of the Atkinson

Table 1  
Coefficients of Equation (3) for  $h_{\text{ACR}}$

M Range	$i$	$a_i$	$b_i$	$M_{ii}$	$c_0$	$c_1$	$c_2$	$c_3$
$\mathbf{M} \leq M_{i1}$	1	0.7497	0.4300	5.744	—	—	—	—
$M_{i1} < \mathbf{M} < M_{i2}$	—	—	—	—	0.7497	0.43000	-0.04875	0.00*
$\mathbf{M} \geq M_{i2}$	2	1.4147	0.2350	7.744	—	—	—	—

For  $h_{\text{SCR}}$ , replace  $a_i$  in the first and third rows with 0.6421 and 1.3071, respectively, and  $c_0$  with 0.6421.

\* $c_3$  is not identically 0.0 but is so small that using 0.0 gives results indistinguishable from those obtained using the actual value.

and Silva, 2000, source model, as determined by the first author; see [Data and Resources](#)) and  $\Delta\sigma_{\text{SCR}} = 185$  bars (found by the first author by inverting data from eight ENA earthquakes, assuming the [Boatwright and Seekins, 2011](#) [BS11] attenuation model), gives this adjustment to the equation for  $h_{\text{ACR}}$ :

$$\log h_{\text{SCR}} = \log h_{\text{ACR}} - 0.1076. \quad (5)$$

The footnote to Table 1 includes this adjustment to the intercept coefficients  $a_1$ ,  $c_0$ , and  $a_2$ .

#### Path Duration

The ground-motion duration used in the stochastic method is a sum of the source duration ( $D_{\text{S}}$ ) and what is called the path duration ( $D_{\text{P}}$ ), which represents the elongation of motion due to wave propagation and scattering effects. Using a recent compilation of data, [Boore and Thompson \(2014\)](#) derived a distance-dependent  $D_{\text{P}}$  function for ACRs that is quite different than the one used in the past. For the convenience of the reader, this new duration function is given in Table 2. (The distance used by Boore and Thompson was  $R_{\text{RUP}}$ , but we now realize that for consistency we should have used  $R_{\text{PS}}$ , as that is the distance used for the other distance-dependent parameters in the stochastic method; we re-evaluated our analysis and find that no adjustment is needed

Table 2

The Path Duration Model for Active Crustal Regions (ACRs) ([Boore and Thompson, 2014](#))

$R_{\text{PS}}$ (km)	$D_{\text{P}}$ (s)
0.0	0.0
7.0	2.4
45.0	8.4
125.0	10.9
175.0	17.4
270.0	34.2

Values for nontabulated distances are given by linear interpolation of the tabulated values (in terms of duration and distance, not logarithms of these quantities). Durations for distance beyond the last tabulated distance are given by  $D_{\text{P}}(R) = D_{\text{P}}(R_{\text{last}}) + 0.156(R - R_{\text{last}})$ .

to the  $D_{\text{P}}$  given in [Boore and Thompson, 2014](#) [and Table 2] if  $R_{\text{PS}}$  is used as the distance measure.) The duration is based on an effective 95%–5% significant duration given by

$$D'_{95} = 2(D_{80} - D_{20}), \quad (6)$$

in which  $D_{20}$  and  $D_{80}$  are the times at which the cumulative integral of acceleration squared reaches 20% and 80% of the final value, respectively (see [Boore and Thompson, 2014](#), for details and the reasons for preferring equation 6 to other parameterizations of duration). The path duration is given by

$$D_{\text{P}} = D'_{95} - D_{\text{S}}. \quad (7)$$

Applying the same analysis to a recent extensive dataset developed for the Pacific Earthquake Engineering Research (PEER) Center's NGA-East project (see [Data and Resources](#)), we find that in general  $D_{\text{P}}$  from the NGA-East database is larger than from the NGA-West 2 database.

The difference in  $D_{\text{P}}$  for ACRs and SCRs is shown in Figure 3, which plots  $D_{\text{P}}$  as a function of  $R_{\text{PS}}$ . Also shown in Figure 3 is the new path duration function we propose for SCRs, as well as the [Boore and Thompson \(2014\)](#) function and median data values for ACRs (path durations for individual records for  $\mathbf{M}$  4–5 are included to illustrate the scatter in the data). In addition, the path duration proposed by [Atkinson and Boore \(1995; AB95\)](#), which has been used in several simulations of ENA ground motions (e.g., AB95, [Atkinson and Boore, 2006, 2007](#)) is also shown. The new function that we suggest be used for SCRs is given in Table 3. The longer durations for SCRs than for ACRs might be a result of the smaller intrinsic attenuation in the cooler crust, which allows the scattered waves to prolong the duration of shaking.

Because the essence of the stochastic method of ground-motion simulation is to spread the energy radiated from the source over a duration given by the sum of the source and path durations, longer path durations will result in smaller amplitude GMIMs. The difference in motions from the AB95 path duration and the one proposed in this article is illustrated in Figure 4, which shows PSA for  $T = 0.1$  s and  $\mathbf{M}$  4.5 and  $\mathbf{M}$  7.5 for the BS11 attenuation model. The 102-bar stress parameter used in the simulations came from an inversion of data from eight ENA earthquakes with magnitudes near  $\mathbf{M}$  5, using the BS11 attenuation model, the AB95 path durations, the crustal amplifications for a site

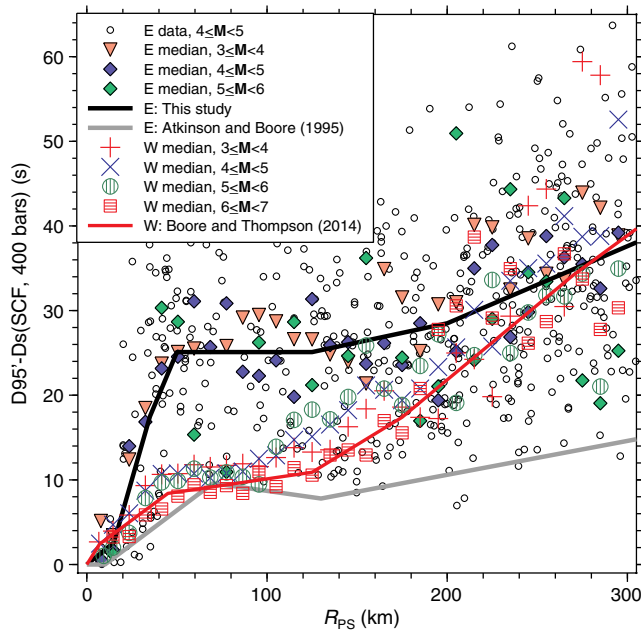


**Figure 3.** The medians in various magnitude ( $M$ ) and point-source distance ( $R_{PS}$ ) bins of the path duration  $D_P = D_{0.5} - D_S$  for data both from eastern North America (E) and ACRs (W). The source duration  $D_S$  is given by  $1/f_c$ , in which the corner frequency  $f_c$  is given by the single-corner frequency model with a stress parameter of 400 bars. Guided primarily by the medians for the  $M$  4–5 range (the individual data points for this magnitude range are shown by the small open circles), we subjectively derived a path duration function consisting of joined linear segments (this study). For comparison, the  $D_P$  used in some previous simulations of motions in eastern North America (Atkinson and Boore, 1995) and the recent path duration for ACRs (Boore and Thompson, 2014) are also shown. The color version of this figure is available only in the electronic edition.

with  $V_{S30} = 2000$  m/s (described below), and the data and methodology of Boore (2012). As shown in Figure 4, the effect of using the new duration is to reduce the motions by a factor as small as 0.65, keeping all other parameters the same. Using the same model except for the new path duration, the stress parameter from the inversion of the same data is 185 bars; and, as shown in Figure 4, simulations with this stress parameter and the new path durations are very similar to those for 102 bars and the older path duration for  $M$  4.5, as they should be. The agreement is not as good for  $M$  7.5, because the relative contributions of source and path durations change with magnitude, such that the effect of path duration on the simulated motions becomes less important as magnitude increases.

### Crustal Amplification

Crustal amplifications account for the increase in the amplitude of the shear waves as they travel from the source region to the Earth's surface. Boore and Joyner (1997; BJ97) presented these amplifications, without attenuation, for two average velocity models represented by gradients of the shear-wave velocity with depth. The two models corresponded to

**Table 3**  
The Path Duration Model for Stable Continental Regions (SCRs)

$R_{PS}$ (km)	$D_P$ (s)
0.0	0.0
15.0	2.6
35.0	17.5
50.0	25.1
125.0	25.1
200.0	28.5
392.0	46.0
600.0	69.1

Values for nontabulated distances are given by linear interpolation of the tabulated values (in terms of duration and distance, not logarithms of these quantities). Durations for distance beyond the last tabulated distance are given by  $D_P(R) = D_P(R_{last}) + 0.111(R - R_{last})$ .

velocities in ACRs and SCR, with  $V_{S30}$  of 618 m/s and 2.8 km/s, respectively. The amplifications were computed using the square-root impedance (SRI) method (Boore, 2013). We present here updates to these amplifications.

For ACRs, we have modified the BJ97 crustal amplifications to reflect an improved density–velocity relationship, with smaller densities for lower velocities (see Data and Resources). The new amplifications are given in Table 4.

For SCR, we provide amplifications in Table 5 for sites with two values of  $V_{S30}$ : 2.0 and 3.0 km/s.  $V_{S30} = 3.0$  km/s was chosen as the reference condition in the PEER NGA-East project (C. Goulet, written comm., 2014; Hashash *et al.*, 2014). On the other hand, no sites in the PEER NGA-East database have velocities as high as 3.0 km/s, and it appears that  $V_{S30} = 2.0$  km/s is a more reasonable value for an average rock site in ENA.

Because the amplifications are usually used in conjunction with a multiplicative exponential diminution operator, we find that it is best to obtain amplifications for nontabulated frequencies by the interpolation function  $\ln A(f) = \ln A_j + s(f - f_j)$ , in which  $f$  is between the tabulated frequencies  $f_j$  and  $f_{j+1}$ , and  $s = \ln(A_{j+1}/A_j)/(f_{j+1} - f_j)$ .

Crustal amplifications for a site with  $V_{S30} = 3.0$  km/s are shown in Figure 5. One model (vms1cnaCG) is from the NGA-East project; the other is a revision of the BJ97 very-hard-rock model, with the surface layers replaced by a single 300 m thick layer with  $V_{S30} = 3.0$  km/s (Fig. 5a). Figure 5b shows amplifications for the two models for angles of incidence (aoi) of  $0^\circ$ . The amplification for the modified BJ97 velocity model is also shown for an aoi of  $40^\circ$ . Although this, or even a greater aoi, may be a more realistic aoi for waves in very hard rock approaching the Earth's surface, Boore (2013) shows that the SRI amplifications are consistently smaller than those from full resonant (FR) calculations for smooth gradient style profiles, by about 5%–20%. Boore (2013) also shows that the SRI amplifications for aoi =  $0^\circ$  are between the FR amplifications with aoi of  $30^\circ$  and  $45^\circ$  (for the BJ97 rock model for ACRs). For this reason, we use the SRI

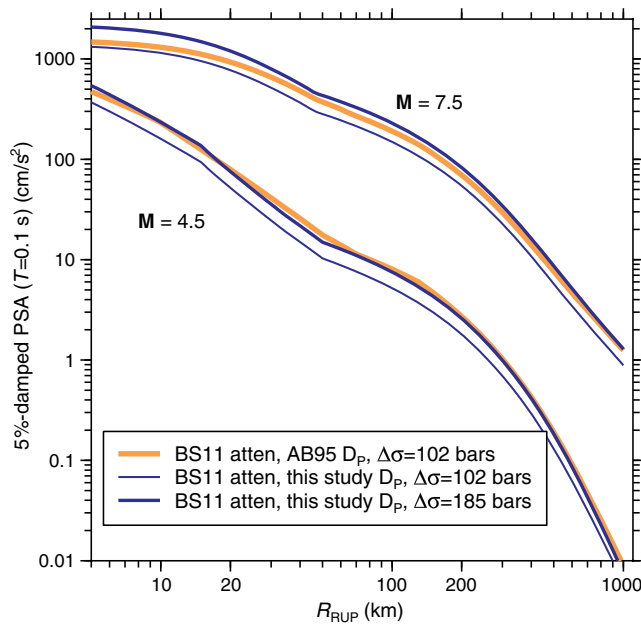


**Figure 4.** Simulated motions for stable continental regions (SCRs) using different path duration ( $D_p$ ; Atkinson and Boore, 1995 [AB95]) and stress parameters, all of which used the Boatwright and Seekins (2011; BS11) attenuation parameters. A feature of this figure that is aside from the main topics of this article is the difference in apparent geometrical spreading of the motions for the two magnitudes ( $M$ ); this is largely due to the finite-fault effect. For a given rupture distance ( $R_{RUP}$ ), the simulations were computed for a point-source distance ( $R_{PS}$ ) given by equations (1), (3), and (5).  $R_{PS}$  is relatively constant for  $R_{RUP} < h$ , and this leads to a plateau in ground motion at close distances when plotted against  $R_{RUP}$ . Because  $h$  increases with  $M$ , the plateau extends to greater values of  $R_{RUP}$  for larger  $M$  earthquakes than for smaller  $M$  events, thus leading to the apparent difference in geometrical spreading seen in the figure (for this figure,  $h_{SCR} = 1.3$  km and  $h_{SCR} = 17.7$  km for  $M = 4.5$  and  $M = 7.5$ , respectively). The color version of this figure is available only in the electronic edition.

amplifications corresponding to the BJ97 very-hard-rock model with  $aoi = 0^\circ$  for our SCR crustal amplifications (Table 5). These have a maximum amplification of 1.15, but as shown in Figure 5, attenuation will decrease this significantly (to 1.11 for  $\kappa = 0.006$  s, the value used for the reference rock in the PEER NGA-East project).

The crustal amplifications given in Table 5 for a site with  $V_{S30} = 2.0$  km/s are based on a velocity profile constructed by replacing the top 300 m of the standard profile of BJ97 with a 30 m thick layer with a constant velocity of 2000 m/s, underlain by material with a linear gradient that connected the 2000 m/s value at 30 m with the 3000 m/s value at a depth of 300 m in the BJ97 very-hard-rock profile. The crustal amplifications were computed with the same method and assumption about the angle of incidence as used for the  $V_{S30} = 3.0$  km/s amplifications.

### Random-Vibration Parameters

Random-vibration theory provides a very rapid way of simulating GMIMs directly from the ground-motion amplitude

**Table 4**

Crustal Amplification ( $A$ ) and Frequency ( $f$ ) Pairs for ACRs for a Velocity Model for Which  $V_{S30} = 618$  m/s

$f$	$A$
0.001	1.00
0.009	1.01
0.025	1.03
0.049	1.06
0.081	1.10
0.150	1.19
0.370	1.39
0.680	1.58
1.110	1.77
2.360	2.24
5.250	2.75
60.30	4.49
100.0	4.49

Modified from table 3 in Boore and Joyner (1997).

**Table 5**

Crustal Amplification ( $A$ ) and Frequency ( $f$ ) Pairs for SCRs for Velocity Models for Which  $V_{S30} = 2.0$  km/s and  $V_{S30} = 3.0$  km/s

$f$	$A(V_{S30} = 2 \text{ km/s})$	$f$	$A(V_{S30} = 3 \text{ km/s})$
0.010	1.000	0.001	1.000
0.015	1.008	0.008	1.003
0.032	1.015	0.023	1.010
0.054	1.026	0.040	1.017
0.078	1.038	0.061	1.026
0.111	1.055	0.108	1.047
0.168	1.069	0.234	1.069
0.245	1.086	0.345	1.084
0.387	1.116	0.508	1.101
0.647	1.159	1.090	1.135
0.950	1.202	1.370	1.143
1.556	1.270	1.690	1.148
2.333	1.342	1.970	1.150
3.156	1.386	2.420	1.151
4.333	1.420	—	—
6.126	1.445	—	—
8.662	1.461	—	—
11.376	1.467	—	—
15.164	1.471	—	—
25.586	1.471	—	—

Modified from table 4 in Boore and Joyner (1997).

spectrum, bypassing the need for TD calculations. There are two main issues to be considered in using RVT: (1) the factor to convert an rms measure of the GMIM to the peak GMIM and (2) adjustments needed to compensate for the strongly nonstationary nature of earthquake ground motions, which is inconsistent with some of the fundamental assumptions in RVT.

### rms-to-Peak Factor

Boore (2003) introduced the use of an rms-to-peak factor (R2PF) based on the direct integration of an equation in

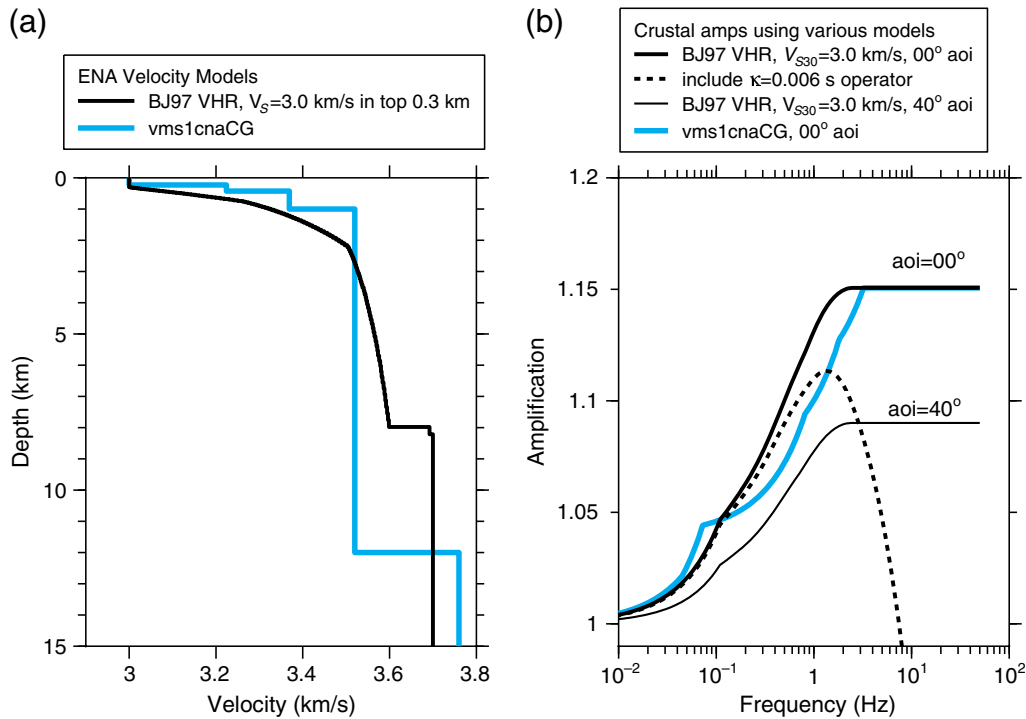


**Figure 5.** (a) Velocity models for a very-hard-rock (VHR) site in eastern North America (ENA): vms1cnaCG and the modified Boore and Joyner (1997; BJ97). See text for an explanation of the models. (b) Amplifications for the two models; the amplification for the BJ97 model is shown for two angles of incidence (aoi), without and with the attenuation operator for aoi = 00°. The color version of this figure is available only in the electronic edition.

Cartwright and Longuet-Higgins (1956), rather than using the more common asymptotic equation. Vanmarcke (1975) proposed a different formulation for the R2PF that includes a term that accounts for the nature of the spectral shape (broadband versus narrowband). Der Kiureghian (1980) simplified Vanmarcke's formulation into a single equation for the peak value cumulative distribution function. The R2PF is computed from the cumulative distribution function as

$$\text{R2PF} \equiv \frac{y_{\max}}{y_{\text{rms}}} = \int_0^{\infty} a \frac{\partial F(a, q, n_z)}{\partial a} da, \quad (8)$$

in which the cumulative distribution function  $F$  is given by equation (2) in Der Kiureghian (1980) (we refer to the R2PF in equation 8 as the DK R2PF because it is easily obtained in the Der Kiureghian paper, unlike the Vanmarcke paper); the shape factor  $q$  is given by

$$q = \sqrt{1 - \frac{m_1^2}{m_0 m_2}}; \quad (9)$$

and the number of zero crossings  $n_z$  (not necessarily an integer) is given by

$$n_z = \frac{1}{\pi} \sqrt{\frac{m_2}{m_0}} D_{\text{EX}}. \quad (10)$$

In equations (9) and (10), the  $m_i$  are spectral moments given by equation (35) in Boore (2003).  $D_{\text{EX}}$  in equation (10) is the

duration of ground-motion excitation (see below). For a given Fourier model of the spectrum of ground motion, we implemented equation (8) by numerical integration, calling a function for  $\partial F/\partial a$  that evaluates equations given by an analytical differentiation of the Der Kiureghian (1980) equation for  $F$ . The integration is stable and rapid, with no singularities in the integrand. The results are included in the output of the relevant SMSIM programs. We do not use the asymptotic R2PF given by equation (4) in Der Kiureghian (1980); instead, we evaluate the equation from which the asymptotic equation was derived. The resulting R2PF cannot be obtained from a convenient closed-form expression, but it should be applicable for a wider range of conditions than that from the asymptotic equation.

#### Time-Domain Versus Random-Vibration Oscillator Responses

We show spectral displacements (SD) for an SCR model using the BS11 attenuation model in Figure 6 and include the path durations in Table 3. The SDs were computed using TD and RV computations. The bottom row shows ratios of the RV/TD simulations. Although the RV simulations using the DK R2PF are closer to the TD simulations (which we take as the correct values) for small magnitudes and short periods than those using the Cartwright and Longuet-Higgins (CL) R2PF, neither R2PF is acceptably accurate. This was recognized by Boore and Joyner (1984), who introduced a

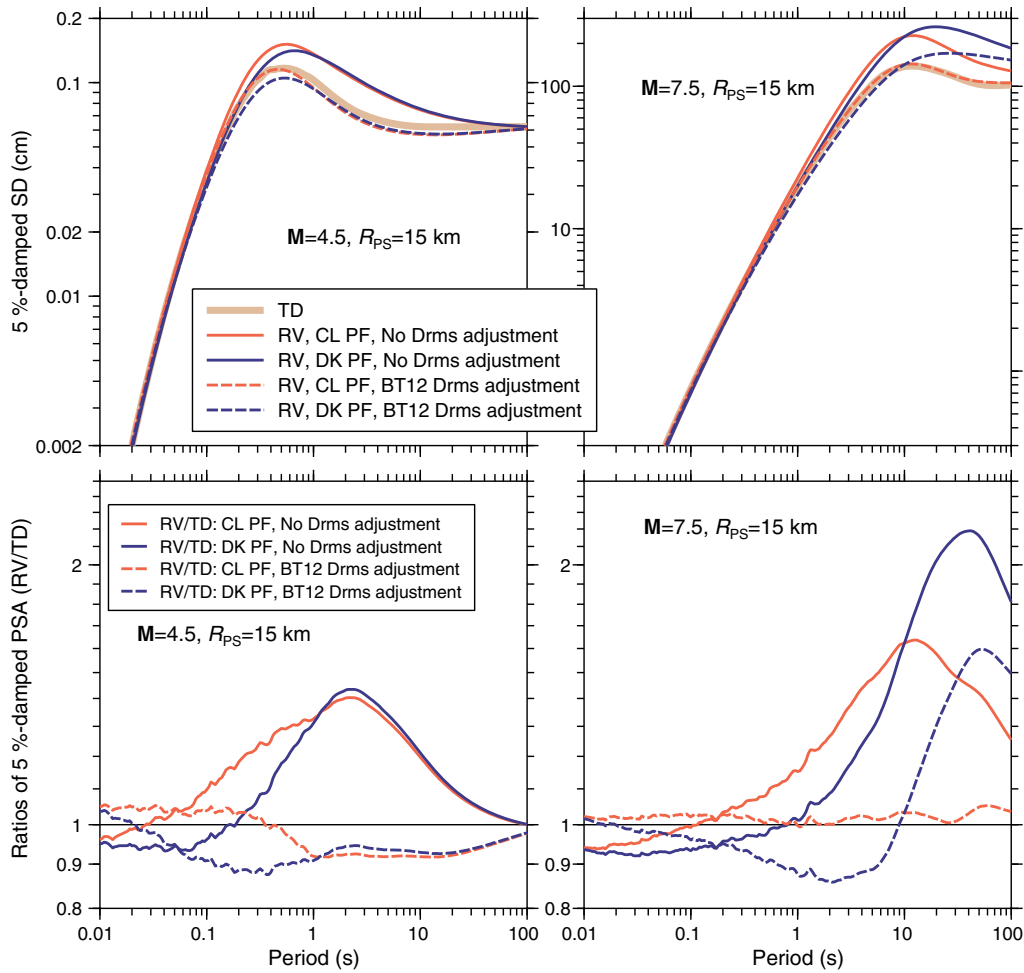


**Figure 6.** (Top) Response spectral displacements (SD) from time-domain (TD) simulations and random-vibration (RV) simulations, without and with adjustments for the duration ( $D_{\text{rms}}$ ) used to compute the root mean square (rms) of the oscillator response. The  $D_{\text{rms}}$  adjustments are those of Boore and Thompson (2012; BT12), not those of this study. The Boatwright and Seekins (2011) attenuation model, the path durations in this study, and a stress parameter of 275 bars were used in the simulations. For the RV simulations, two rms-to-peak factors were used: CL (Cartwright and Longuet-Higgins, 1956) and DK (Der Kiureghian, 1980). (Bottom) Ratios of the RV and TD response spectra. The color version of this figure is available only in the electronic edition.

modification to the duration ( $D_{\text{rms}}$ ) used to compute the rms of an oscillator response. The Boore and Joyner (1984) modifications were refined by Liu and Pezeshk (1999) and further refined by Boore and Thompson (2012; BT12). The modifications are based on a comparison of TD and RV simulations, such as those shown in Figure 6. Because the coefficients in the equation for  $D_{\text{rms}}$  are dependent on both the model parameters used in the simulations and the R2PFs used in the RV simulations, we determined new coefficients for  $D_{\text{rms}}$ . Figure 6 shows the RV simulations with the new model parameters, but using the BT12 coefficients for  $D_{\text{rms}}$ . Although the BT12 coefficients work relatively well for the CL R2PFs (which were used in the RV simulations by BT12), they do not work well for the DK R2PFs. Because of the dependence on the R2PFs and because we have made changes to a number of the model parameters, both for ACRs and SCRs, we determined new sets of coefficients for both regions.

The equation for  $D_{\text{rms}}$  is given in BT12 (their equation 10) and, for convenience, is reproduced as

$$D_{\text{rms}}/D_{\text{EX}} = \left( c_1 + c_2 \frac{1 - \eta^{c_3}}{1 + \eta^{c_3}} \right) \left[ 1 + \frac{c_4}{2\pi\zeta} \left( \frac{\eta}{1 + C_5\eta^{c_6}} \right)^{c_7} \right]. \quad (11)$$

$D_{\text{EX}}$  is the duration of ground motion, independent of oscillator period.  $\text{\textcircled{E}}$  The  $c$  coefficients for a wide range of magnitudes and distances for both ACR and SCR are given in the electronic supplement to this article (they are to be used with the DK R2PFs); the files with the  $c$  coefficients also contain TD/RV for both peak acceleration and peak velocity. Figure 7 shows maps of the ratio TD/RV for an SCR model as a function of period and distance, for the range of magnitudes used in the simulations (M 2–8).  $\text{\textcircled{E}}$  The model parameters are given in the electronic supplement; we consider the model to be the base model used for developing the coefficients

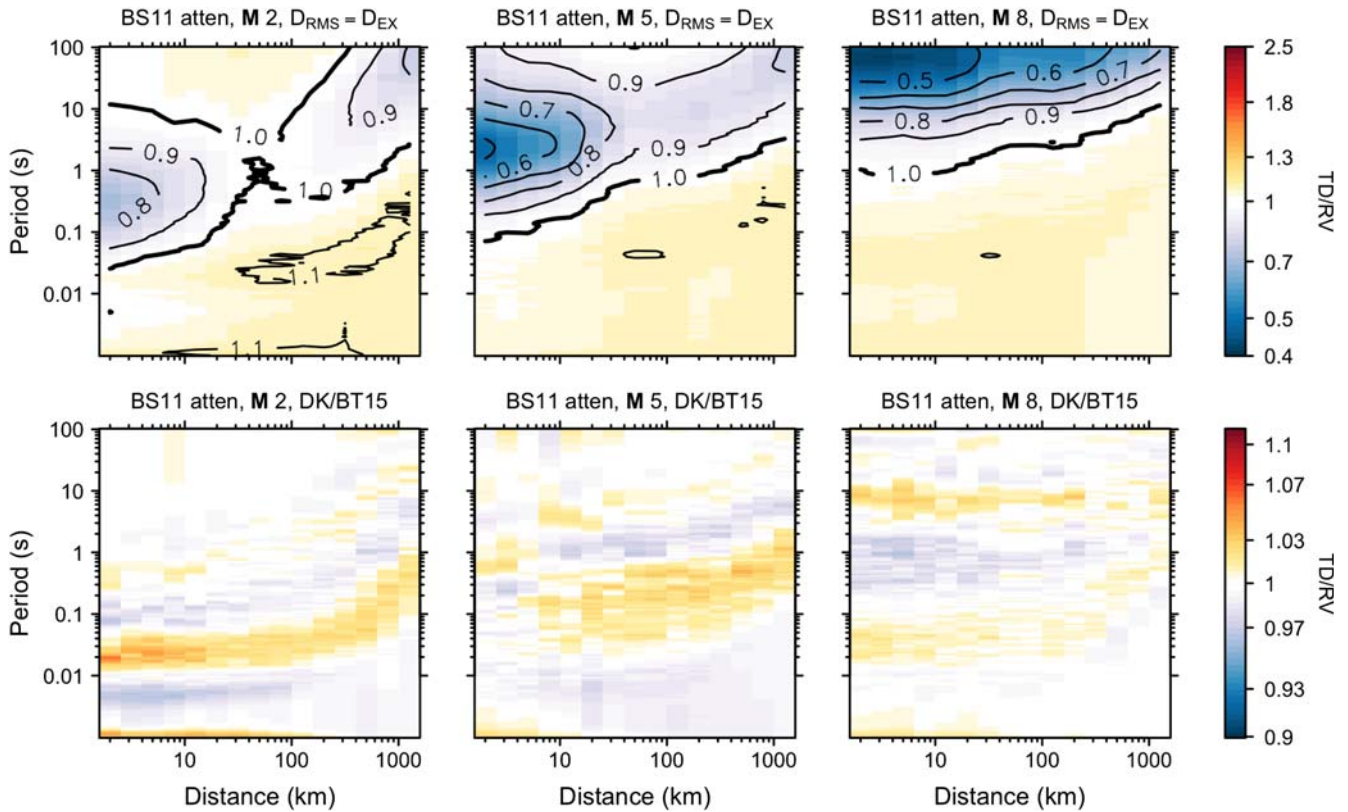


**Figure 7.** Shaded contour plots of the TD/RV ratios for a single-corner-frequency model with 275-bar stress parameter, the Boatwright and Seekins (2011; BS11) geometrical spreading and attenuation, the path durations and crustal amplifications given in Tables 3 and 5 (for  $V_{S30} = 3.0$  km/s), and the Der Kiureghian (1980; DK) peak factors for magnitudes ( $M$ ) of 2, 5, and 8. The top row shows the ratios when  $D_{rms} = D_{EX}$  in the RV simulations, and the bottom row shows the TD/RV ratio using the adjustments to  $D_{rms}$  for the BS11 attenuation model given in the  $\text{\textcircled{E}}$  electronic supplement (BT15). Note the change of scale between the top and bottom rows. The color version of this figure is available only in the electronic edition.

in equation (11). It is an SCF source model with a 275-bar stress parameter, the BS11 geometrical spreading and attenuation, and the path durations and crustal amplifications given in Tables 3 and 5 (for  $V_{S30} = 3.0$  km/s). The top row shows the TD/RV ratio with no adjustment to  $D_{rms}$ , and the second row shows the ratio when the RV simulations use the value of  $D_{rms}$  from equation (11), derived by fitting the ratios in the top row of the figure (note the expanded scale compared with that of the top row of graphs). This is a consistency check, showing that the equation for  $D_{rms}$  is working properly.

To explore the sensitivity of the RVT simulations to the coefficients used for determining  $D_{rms}$ , Figure 8 shows the TD/RV ratios for SCR models with somewhat different parameters than the base model used in deriving the coefficients for  $D_{rms}$ . Note the expanded scale used for the graphs (0.9–1.1).  $\text{\textcircled{E}}$  All of the SMSIM parameter files used in the simulations for the TD and the RV simulations are given in the electronic supplement. The first and second rows in Figure 8 are for the base model, but with stress parameters of 69 and 1100 bars, respectively, rather than 275 bars. The results imply that the adjustments to  $D_{rms}$  are relatively insensitive to the stress parameter. The models used in the third and fourth rows depart even farther from the base model. The third row uses the

AB95 path durations and the Atkinson (2004) attenuation model (which decays more rapidly within the first 50 km than does the BS11 model). The graphs in the fourth row use a DCF source model given by Atkinson (1993), but otherwise the parameters are the same as those in the base model. Some of the small ratios in Figure 8 are clipped because of the limited scale used, so we show the ratios for  $M$  5.0 and  $R_{PS} = 20$  km in Figure 9. Except for some situations that are of little interest (e.g., small magnitudes or long periods), the results in Figures 8 and 9 show that relatively accurate results (within about 10% for the examples here) can often be obtained for RV simulations using  $D_{rms}$  values obtained for models that are different than the models for which the simulations are done. In spite of this general conclusion, we note that the ratios shown in Figure 8 are quite different from unity for some regions of magnitude, distance, and period space. To understand the reasons for this difference, we made a number of graphs of the various factors that are used in the RV simulations. Although it is difficult to draw general conclusions, it seems that differences in path duration between the model being considered and the model used to derive the coefficients used to obtain  $D_{rms}$  are of primary importance. These differences can lead to significant differences in the number of zero crossings

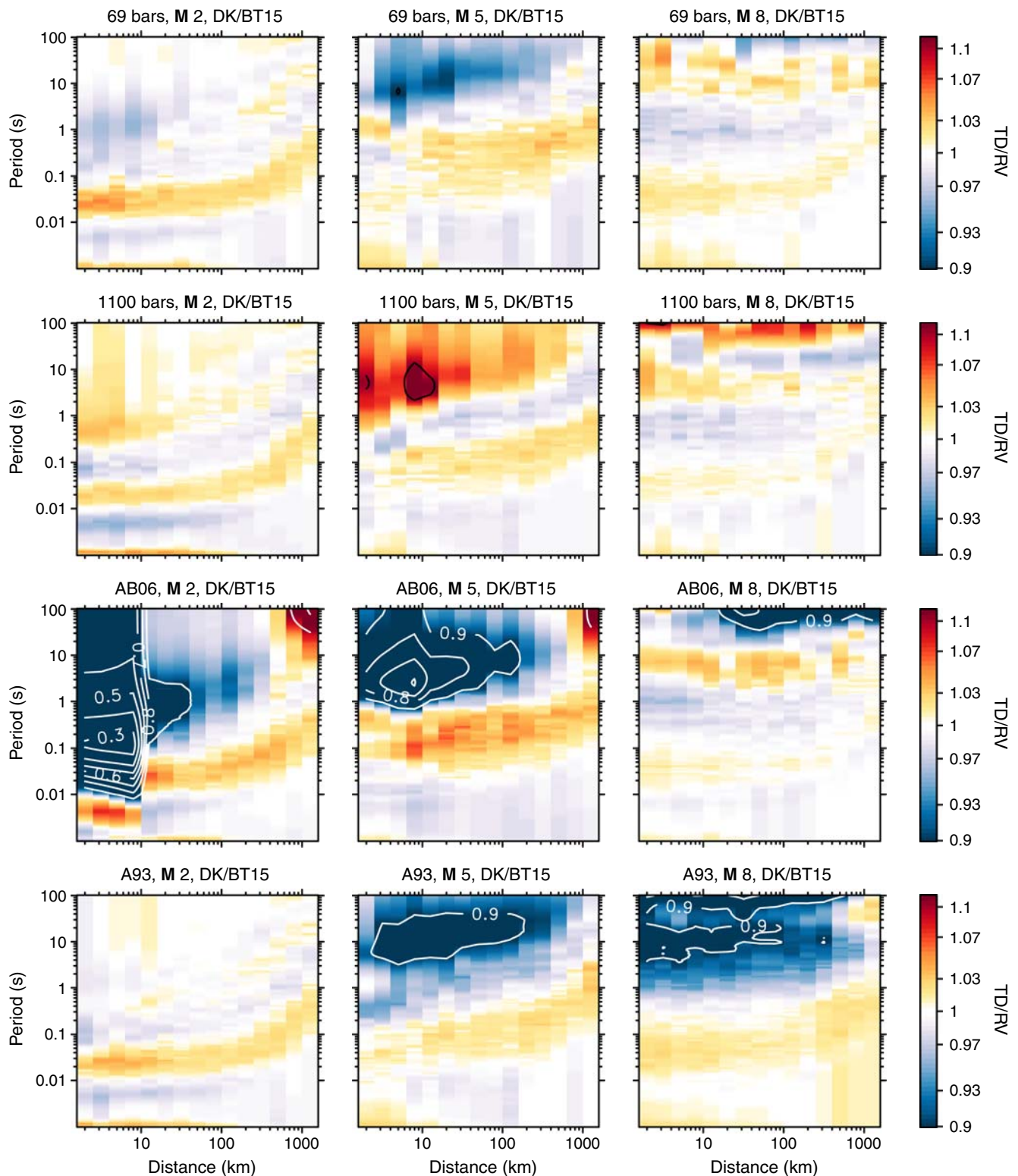


**Figure 8.** Shaded contour plots of the TD/RV ratios for various models not used to derive the coefficients used in the RVT simulations. The top two rows used the same model as used to derive the  $D_{\text{rms}}$  coefficients, except that the stress parameters were factors of 4 less than and greater than the 275 bar used in those simulations. The third row used a single-corner-frequency source with 400-bar stress parameter, the Atkinson (2004) attenuation, and the Atkinson and Boore (1995) path durations. The bottom row used the Atkinson (1993; A93) double-corner-frequency source model, but the other parameters were the same as used to derive the  $D_{\text{rms}}$  coefficients. The RV simulations used the Der Kiureghian (1980; DK) rms-to-peak factor (R2PF) and the new coefficients (BT15) for equation (11) given in the  electronic supplement for the Boatwright and Seekins (2011) attenuation model. The color version of this figure is available only in the electronic edition.

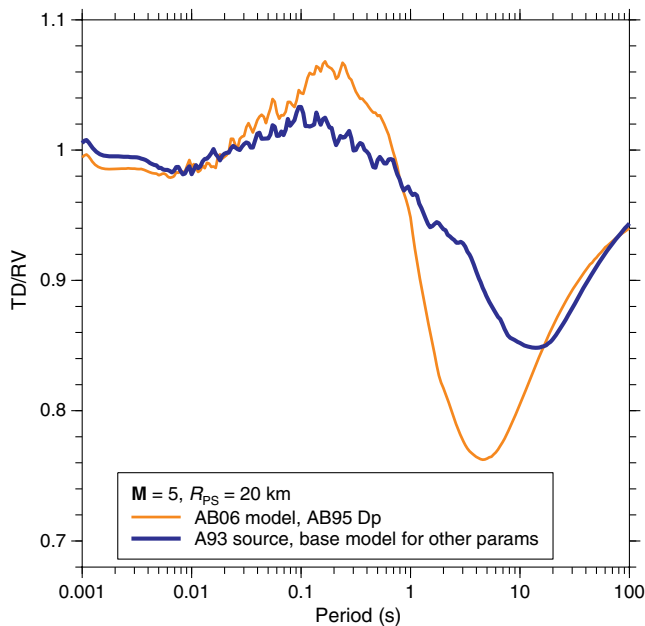


**Figure 9.** Ratios of response spectra from TD and RV simulations for two of the models used in Figure 8, for  $M = 5.0$  and  $R_{PS} = 20$  km. © The model parameters are given in the electronic supplement. The color version of this figure is available only in the electronic edition.

$n_z$  (equation 10), a fundamental variable in determining the R2PF (see equation 8). In general, a smaller  $n_z$  results in a smaller R2PF. One clear example of the importance of the path duration is for the model used in the third row of Figure 8, in which the ratios are significantly less than unity for most periods and for distances less than 10 km and  $M = 2$ , with an abrupt change to ratios closer to unity for distances greater than 10 km. The  $D_P$  function for the AB95 model is 0.0 out to 10 km (the function is shown in Fig. 3); for small earthquakes this implies a very short duration  $D_{EX}$ . The SMSIM implementation of the RVT sets a minimum number of cycles that can contribute to the peak response to be 1.3, which for  $M = 2$  and  $T = 0.15$  s (as an example) is not exceeded for distances less than 10 km. For greater distances, the number of cycles increases rapidly (e.g., it is 9.7 at 12.6 km for  $T = 0.15$  s). For the base model, the number of cycles for  $M = 2$  and  $T = 0.15$  s is 8.2 at 2 km, increasing to 48.7 at 12.6 km. The constant, small value of the number of cycles for distances less than 10 km for the model used in the third row of graphs, compared with the increasing number of cycles with distance for the base model, leads to the large discrepancy in the third row for  $M = 2$ .

### Discussion and Conclusions

Recent adjustments to how the spectrum of the ground motion is specified in the stochastic method of simulating ground motions have required additional updates to the  $D_{rms}$  model to achieve accurate results with RVT. Although

some of these adjustments have been recently published (the generalized DCF model, the new finite-fault correction factor, and the new duration model for active regions), we present additional updates that (1) allow for the ground-motion duration to be modeled in an analogous manner for stable regions and (2) specify crustal amplifications that are consistent with the ongoing NGA-East project. Simultaneously, it was brought to our attention that there may be advantages to using the DK R2PFs in some applications of the stochastic method (E. Rathje, written comm., 2014). Thus, we present new coefficients for computing  $D_{rms}$  that are consistent with these new updates.

Some researchers have modified the stochastic method for site-specific applications where site amplification is modeled using the FR calculation and nonlinearity is modeled with the equivalent-linear method (Kottke and Rathje, 2013). Although the recent TD adjustments presented in this article and elsewhere will affect the specification of the rock motion for site-specific applications, the  $D_{rms}$  correction we provide does not account for the increased duration of the oscillator due to site response resonances. This could be addressed by developing an additional parameter that is a function of the site characteristics to adjust the  $D_{rms}$  equations that we provide here. Alternatively, new  $D_{rms}$  equations can be developed from scratch that account for the impact of the FR site response on the spectral shape and oscillator duration.

### Data and Resources

The durations for ground-motion records from central and eastern North American earthquakes used in this article were provided by C. Goulet (written comm., 2014). The durations were computed from time series collected as part of the Pacific Earthquake Engineering Research (PEER) Next Generation Attenuation (NGA)-East project (<http://peer.berkeley.edu/ngaeast/>; last accessed January 2015). The bulk of the data analysis was done using the program R, available from <http://www.r-project.org/> (last accessed January 2015), and many of the figures were prepared using CoPlot ([www.cohort.com](http://www.cohort.com); last accessed January 2015). The latest version of the Stochastic-Method SIMulation (SMSIM) programs used for the simulations can be obtained from the online software link on <http://www.daveboore.com> (last accessed January 2015); their use is described in Boore (2005). A discussion of the relation between density and velocity is given in [daves\\_notes\\_on\\_relatng\\_density\\_to\\_velocity\\_v1.2.pdf](http://www.daveboore.com/daves_notes_on_relatng_density_to_velocity_v1.2.pdf), available from [http://www.daveboore.com/daves\\_notes.html](http://www.daveboore.com/daves_notes.html) (last accessed January 2015). The determination of the stress parameter equivalent to the Atkinson and Silva (2000) source model is given in [What\\_SCF\\_stress\\_param\\_is\\_consistent\\_with\\_the\\_AS00\\_source\\_model.pdf](http://www.daveboore.com/What_SCF_stress_param_is_consistent_with_the_AS00_source_model.pdf), available from [http://www.daveboore.com/daves\\_notes.html](http://www.daveboore.com/daves_notes.html) (last accessed January 2015). Yenier and Atkinson (2015) is an unpublished report based on Yenier (2015).

## Acknowledgments

This article was prepared as an account of work sponsored by an agency of the U.S. Government. Neither the U.S. Government nor any agency thereof, nor any of their employees, makes any warranty, expressed or implied, or assumes any legal liability or responsibility for any third party's use, or the results of such use, of any information, apparatus, product, or process disclosed in this report, or represents that its use by such third party would not infringe privately owned rights. The views expressed in this article are not necessarily those of the U.S. Nuclear Regulatory Commission. We thank Ellen Rathje for discussions related to the root mean square (rms)-to-peak factor and for her program in which she computed the factor directly from equation (2) in Der Kiureghian (1980). We also thank Christine Goulet for the duration database, as well as Carola Di Alessandro, Ellen Rathje, Emrah Yenier, and Hamid Zafarani for useful comments on the article.

## References

- Atkinson, G. M. (1993). Earthquake source spectra in eastern North America, *Bull. Seismol. Soc. Am.* **83**, 1778–1798.
- Atkinson, G. M. (2004). Empirical attenuation of ground-motion spectral amplitudes in southeastern Canada and the northeastern United States, *Bull. Seismol. Soc. Am.* **94**, 1079–1095.
- Atkinson, G. M., and D. M. Boore (1995). Ground motion relations for eastern North America, *Bull. Seismol. Soc. Am.* **85**, 17–30.
- Atkinson, G. M., and D. M. Boore (2003). Empirical ground-motion relations for subduction zone earthquakes and their application to Cascadia and other regions, *Bull. Seismol. Soc. Am.* **93**, 1703–1729.
- Atkinson, G. M., and D. M. Boore (2006). Earthquake ground-motion prediction equations for eastern North America, *Bull. Seismol. Soc. Am.* **96**, 2181–2205.
- Atkinson, G. M., and D. M. Boore (2007). Erratum to Earthquake ground-motion prediction equations for eastern North America, *Bull. Seismol. Soc. Am.* **97**, 1032.
- Atkinson, G. M., and W. Silva (2000). Stochastic modeling of California ground motions, *Bull. Seismol. Soc. Am.* **90**, 255–274.
- Baltay, A. S., and T. C. Hanks (2014). Understanding the magnitude dependence of PGA and PGV in NGA-West2 data, *Bull. Seismol. Soc. Am.* **104**, 2851–2865, doi: [10.1785/0120130283](https://doi.org/10.1785/0120130283).
- Beresnev, I. A., and G. M. Atkinson (1998). FINSIM—A FORTRAN program for simulating stochastic acceleration time histories from finite faults, *Seismol. Res. Lett.* **69**, 27–32.
- Boatwright, J., and L. Seekins (2011). Regional spectral analysis of three moderate earthquakes in northeastern North America, *Bull. Seismol. Soc. Am.* **101**, 1769–1782.
- Boore, D. M. (1983). Stochastic simulation of high-frequency ground motions based on seismological models of the radiated spectra, *Bull. Seismol. Soc. Am.* **73**, 1865–1894.
- Boore, D. M. (2003). Simulation of ground motion using the stochastic method, *Pure Appl. Geophys.* **160**, 635–675.
- Boore, D. M. (2005). SMSIM—Fortran programs for simulating ground motions from earthquakes: Version 2.3—A revision of OFR 96-80-A, *U.S. Geol. Surv. Open-File Rept. 00-509*, 55 pp.
- Boore, D. M. (2009). Comparing stochastic point-source and finite-source ground-motion simulations: SMSIM and EXSIM, *Bull. Seismol. Soc. Am.* **99**, 3202–3216.
- Boore, D. M. (2012). Updated determination of stress parameters for nine well-recorded earthquakes in eastern North America, *Seismol. Res. Lett.* **83**, 190–199.
- Boore, D. M. (2013). The uses and limitations of the square-root impedance method for computing site amplification, *Bull. Seismol. Soc. Am.* **103**, 2356–2368.
- Boore, D. M. (2014). What do data used to develop ground-motion prediction equations tell us about motions near faults? *Pure Appl. Geophys.* **171**, 3023–3043.
- Boore, D. M., and W. B. Joyner (1984). A note on the use of random vibration theory to predict peak amplitudes of transient signals, *Bull. Seismol. Soc. Am.* **74**, 2035–2039.
- Boore, D. M., and W. B. Joyner (1997). Site amplifications for generic rock sites, *Bull. Seismol. Soc. Am.* **87**, 327–341.
- Boore, D. M., and E. M. Thompson (2012). Empirical improvements for estimating earthquake response spectra with random-vibration theory, *Bull. Seismol. Soc. Am.* **102**, 761–772.
- Boore, D. M., and E. M. Thompson (2014). Path durations for use in the stochastic-method simulation of ground motions, *Bull. Seismol. Soc. Am.* **104**, 2541–2552, doi: [10.1785/0120140058](https://doi.org/10.1785/0120140058).
- Boore, D. M., C. Di Alessandro, and N. A. Abrahamson (2014). A generalization of the double-corner-frequency source spectral model and its use in the SCEC BBP Validation Exercise, *Bull. Seismol. Soc. Am.* **104**, 2387–2398.
- Boore, D. M., J. P. Stewart, E. Seyhan, and G. M. Atkinson (2014). NGA-West 2 equations for predicting PGA, PGV, and 5%-damped PSA for shallow crustal earthquakes, *Earthq. Spectra* **30**, 1057–1085.
- Cartwright, D. E., and M. S. Longuet-Higgins (1956). The statistical distribution of the maxima of a random function, *Proc. Roy. Soc. Lond.* **237**, 212–232.
- Der Kiureghian, A. (1980). Structural response to stationary excitation, *J. Eng. Mech. Div.* **106**, 1195–1213.
- Frankel, A. (2009). A constant stress-drop model for producing broadband synthetic seismograms: Comparison with the Next Generation Attenuation relations, *Bull. Seismol. Soc. Am.* **99**, 664–680.
- Graves, R. W., and A. Pitarka (2010). Broadband time history simulation using a hybrid approach, *Bull. Seismol. Soc. Am.* **100**, 2095–2123.
- Hanks, T. C., and R. K. McGuire (1981). The character of high-frequency strong ground motion, *Bull. Seismol. Soc. Am.* **71**, 2071–2095.
- Hashash, Y., A. Kottke, K. Campbell, B. Kim, C. Moss, S. Nikolaou, E. Rathje, W. Silva, and J. Stewart (2014). Reference rock site condition for central and eastern North America, *Bull. Seismol. Soc. Am.* **104**, 684–701, doi: [10.1785/0120130132](https://doi.org/10.1785/0120130132).
- Kottke, A. R., and E. M. Rathje (2008). Technical Manual for Strata, *PEER Rept. 2008/10*, Pacific Earthquake Engineering Research Center, University of California at Berkeley, 84 pp.
- Kottke, A. R., and E. M. Rathje (2013). Comparison of time series and random vibration theory site response methods, *Bull. Seismol. Soc. Am.* **103**, 2111–2127.
- Liu, L., and S. Pezeshk (1999). An improvement on the estimation of pseudoresponse spectral velocity using RVT method, *Bull. Seismol. Soc. Am.* **89**, 1384–1389.
- Motazedian, D., and G. M. Atkinson (2005). Stochastic finite-fault modeling based on a dynamic corner frequency, *Bull. Seismol. Soc. Am.* **95**, 995–1010.
- Rathje, E. M., and M. C. Ozbey (2006). Site-specific validation of random vibration theory-based seismic site response analysis, *J. Geotech. Geoenviron. Eng.* **132**, 911–922.
- Stewart, J. P., J. Douglas, M. Javanbarg, Y. Bozorgnia, N. A. Abrahamson, D. M. Boore, K. W. Campbell, E. Delavaud, M. Erdik, and P. J. Stafford (2014). Selection of ground motion prediction equations for the Global Earthquake Model, *Earthq. Spectra* **30**, doi: [10.1193/013013EQS017M](https://doi.org/10.1193/013013EQS017M).
- Toro, G. R. (2002). Modification of the Toro et al. (1997) attenuation relations for large magnitudes and short distances, *Risk Engineering, Inc. Report*, available from [http://www.riskeng.com/downloads/attenuation\\_equations](http://www.riskeng.com/downloads/attenuation_equations) (last accessed 10 May 2014).
- Vanmarcke, E. H. (1975). Distribution of first-passage time for normal stationary random processes, *J. Appl. Mech. Trans. ASME* **42**, 215–220.
- Yenier, E. (2015). Regionally-adjustable generic ground-motion prediction equation, *Ph.D. Thesis*, Department of Earth Sciences, University of Western Ontario, London, Ontario, Canada, 174 pp.
- Yenier, E., and G. M. Atkinson (2014). Equivalent point-source modeling of moderate-to-large magnitude earthquakes and associated ground-motion saturation effects, *Bull. Seismol. Soc. Am.* **104**, 1458–1478.

## Appendix

Given the  $a$  and  $b$  coefficients in equation (3), the four  $c$  coefficients are determined by requiring that the value and slope of the cubic equal the value and slope of lines 1 and 2 when  $\mathbf{M} = M_{t1}$  and  $\mathbf{M} = M_{t2}$ , respectively. This gives the following equations for the  $c$  coefficients:

$$c_0 = a_1, \quad (\text{A1})$$

$$c_1 = b_1, \quad (\text{A2})$$

$$c_2 = \frac{2\Delta a}{\Delta \mathbf{M}^2} - \frac{0.5}{\Delta \mathbf{M}} [3b_1 + b_2], \quad (\text{A3})$$

and

$$c_3 = \frac{0.5}{\Delta \mathbf{M}^2} \left\{ \Delta b - 2 \left[ \frac{\Delta a}{\Delta \mathbf{M}} - b_1 \right] \right\}, \quad (\text{A4})$$

in which

$$\Delta a = a_2 - a_1, \quad (\text{A5})$$

$$\Delta b = b_2 - b_1, \quad (\text{A6})$$

and

$$\Delta \mathbf{M} = M_{t2} - M_{t1}. \quad (\text{A7})$$

U.S. Geological Survey  
MS 977  
345 Middlefield Road  
Menlo Park, California 94025  
boore@usgs.gov  
(D.M.B.)

Department of Geological Sciences  
San Diego State University  
San Diego, California 92182  
ethompson@mail.sdsu.edu  
(E.M.T.)

Manuscript received 17 September 2014;  
Published Online 3 March 2015